JOURNAL OF GUIDANCE, CONTROL, AND DYNAMICS
Vol. 27, No. 5, September–October 2004

Adaptive Sliding Mode Control Design for a Hypersonic Flight Vehicle

Haojian Xu
University of Southern California, Los Angeles, California 90089
Maj D. Mirmirani
California State University, Los Angeles, California 90032
and
Petros A. Ioannou
University of Southern California, Los Angeles, California 90089

A multi-input/multi-output adaptive sliding controller is designed and analyzed for the longitudinal dynamics of a generic hypersonic air vehicle. This vehicle model is nonlinear, multivariable, and unstable and includes uncertain parameters. Simulation studies are conducted for trimmed cruise conditions of 110,000 ft and Mach 15 where the responses of the vehicle to a step change in altitude and airspeed are evaluated. The commands are 100-ft/s step velocity and 2000-ft step altitude. The controller is evaluated for robustness with respect to parameter uncertainties using simulations. Simulation studies demonstrate that the proposed controller is robust with respect to parametric uncertainty and meets the performance requirements with relatively low-amplitude control inputs.

Nomenclature

a	=	combined uncertainty parameter, $\text{ft} \cdot \text{s}^2$
b	=	combined uncertainty parameter, ft^3/s
C_D	=	drag coefficient
C_L	=	lift coefficient
$C_M(q)$	=	moment coefficient due to pitch rate
$C_M(\alpha)$	=	moment coefficient due to angle of attack
$C_M(\delta_e)$	=	moment coefficient due to elevator deflection

Haojian Xu received his B.S. degree from Nanjing University of Aeronautics and Astronautics, the People's Republic of China, in 1990 and M.S. and Ph.D. degrees in electrical engineering from the University of Southern California, Los Angeles, California, in 1999 and 2002, respectively. From 1990 to 1997, he worked as an engineer at the Beijing Aerospace Automatic Control Institute, China Academy of Launch Vehicle Technology. He is currently working as a postdoctoral research associate in the Department of Electrical Engineering, University of Southern California. He has served as a reviewer for various journals and conferences. His current research interests include robust adaptive control, nonlinear system control with application to high-performance aircraft, control of unknown systems using neural networks, and system identification and control of hard disk drive systems. Member AIAA. He may be contacted at haojian@usc.edu.

Maj Dean Mirmirani received his B.S. degree from Tehran Polytechnic in 1969, and M.S. and Ph.D. degrees in mechanical engineering from the University of California, Berkeley, in 1971 and 1976, respectively. Before joining the Department of Mechanical Engineering at California State University, Los Angeles, in 1981, he was an academic visitor for one year at the Department of Electrical Engineering, Imperial College of Science and Technology, London. Currently he is a professor and Chairman of the Mechanical Engineering Department and Director of the Multidisciplinary Flight Dynamics and Control Laboratory at California State University, Los Angeles, which is funded by NASA Dryden Flight Research Center and the Air Force Office of Scientific Research. His research interests are in the areas of multidisciplinary modeling and analysis of flight vehicles, control of hypersonic airbreathing flight vehicles, and aeroservoelasticity. M. D. Mirmirani is the recipient of the 2002–2003 California State University Los Angeles Outstanding Professor Award and a member of AIAA. His e-mail address is mmirmir@exchange.calstatela.edu.

Petros A. Ioannou received his B.Sc. degree with first class honors from University College, London, England, in 1978 and the M.S. and Ph.D. degrees from the University of Illinois, Urbana, Illinois, in 1980 and 1982, respectively. In 1982, he joined the Department of Electrical Engineering Systems, University of Southern California, Los Angeles, California. He is currently a professor in the same department and Director of the Center of Advanced Transportation Technologies. His research interests are in the areas of adaptive control, neural networks, nonlinear systems, vehicle dynamics and control, intelligent transportation systems, and marine transportation. He was Visiting Professor at the University of Newcastle, Australia in the fall of 1988, the Technical University of Crete in summer of 1992, and served as Dean of the School of Pure and Applied Science at the University of Cyprus in 1995. In 1984 he was a recipient of the Outstanding IEEE Transactions Paper Award and the recipient of 1985 Presidential Young Investigator Award. He is the author/coauthor of 5 books and more than 150 research papers in the area of controls, neural networks, nonlinear dynamical systems, and intelligent transportation systems. His e-mail address is ioannou@usc.edu.

Presented as Paper AAS 01-240 at the AAS/AIAA 11th Space Flight Mechanics Meeting, Santa Barbara, February 2001; received 19 February 2002; revision received 15 August 2003; accepted for publication 5 January 2004.

C_T = thrust coefficient
$\bar{c}$ = mean aerodynamic chord, ft
D = drag, lbf
h = altitude, ft
I_{yy} = moment of inertia, slug $\cdot$ ft^2
k_h, k_q = observer sliding gains, 1/s
k_1, k_2 = controller sliding gains, 1/s
k_α = observer sliding gain
k_γ = observer sliding gain, rad/ft $\cdot$ s
L = lift, lbf
M = Mach number
M_{yy} = pitching moment, lbf $\cdot$ ft
m = mass, slug
q = pitch rate, rad/s
R_E = radius of the Earth, ft
r = radial distance from Earth's center, ft
S = reference area, ft^2
T = thrust, lbf
V = velocity, ft/s
α = angle of attack, rad
β = throttle setting
γ = flight-path angle, rad
δ_e = elevator deflection, rad
η_1, η_2 = observer damping coefficients, 1/s
η_3 = observer damping coefficient, rad/ft $\cdot$ s
η_4 = observer damping coefficient
λ_1, λ_2 = bandwidth of tracking error dynamics, 1/s
μ = gravitational constant
ρ = density of air, slug/ft^3
Φ_1, Φ_2 = boundary-layer widths, ft/s^3

Introduction

HYPERSONIC air vehicles are sensitive to changes in flight condition as well as physical and aerodynamic parameters due to their design and flight conditions of high altitudes and Mach numbers. For example, at cruise flight at altitude of 110,000 ft and Mach 15, a 1-deg increase in angle of attack produces a load factor of about 0.33 g. Furthermore, it is difficult to measure or estimate the atmospheric properties and aerodynamic characteristics at the hypersonic flight altitude. As a result, modeling inaccuracies can result and can have strong adverse effects on the performance of air vehicle's control systems. Therefore, robust control has been the main technique used for hypersonic flight control.[1,2]

The sliding mode control method provides a systematic approach to the problem of maintaining stability and consistent performance in the face of modeling imprecision. The main advantage of sliding mode control is that the system's response remains insensitive to model uncertainties and disturbances.[3,4] The most completely developed area of sliding mode control is for single-input/single-output systems (SISO).[3] In Ref. 4, SISO sliding mode control is extended to a class of nonlinear multi-input/multi-output (MIMO) systems. Although the technique has good robustness properties, pure sliding mode control presents drawbacks that include large control authority requirements and chattering. The performance of pure sliding mode control can be improved by coupling it with an online parameter estimation scheme.[5] Also, a sliding mode controller can be implemented only if full state feedback is available, a requirement not readily achieved in a hypersonic flight. The design of a state observer for the unmeasurable states based on sliding modes has been proposed in Ref. 6, where it is shown that sliding mode observers have inherent robustness properties in the face of parametric uncertainty and measurement noise. An adaptive sliding mode controller combined with an observer was applied to a SISO magnetic suspension system in Ref. 7 and to a linear MIMO robotic system in Ref. 8.

In this paper, design of a MIMO adaptive controller for a hypersonic air vehicle based on the sliding mode control technique is presented. The plant is the longitudinal model of a generic hypersonic air vehicle.[1,2] This model is nonlinear, multivariable, and unstable with seven uncertain inertial and aerodynamic parameters. The open-loop dynamics of the air vehicle exhibits unstable short-period and height modes, as well as a lightly damped phugoid mode. The control design described in the following sections consists of four steps. First, full-state feedback is applied to linearize the dynamics of the air vehicle with respect to air speed V and altitude h. Next, a pure sliding mode controller is designed. An adaptive sliding mode controller is then designed to improve performance in the presence of parametric uncertainty. In addition, a sliding mode observer is designed to estimate the angle of attack and the flight-path angle, which are difficult to measure in a hypersonic flight. [Although with global positioning system- (GPS-) aided inertial navigation it is reasonable to assume that the flight-path angle could be calculated from the rate change of altitude and velocity.] However, in this study we consider the worst case where neither the flight-path angle measurement nor its calculated value is available. Finally, the overall controller is synthesized by combining the adaptive controller with the observer. Simulation studies are conducted for trimmed cruise conditions of 110,000 ft and Mach 15 to evaluate the response of the vehicle to a step change of 2000 ft in altitude and 100 ft/s in airspeed. Parameter uncertainties are included in the inertial and aerodynamic coefficients and are allowed to take their maximum possible deviation in the simulation studies. The results demonstrate that at the trimmed flight conditions used for the simulations the combined adaptive sliding controller is robust with respect to parametric uncertainty and provides good performance with limited control authority.

Hypersonic Air Vehicle Model

A model for the longitudinal dynamics of a generic hypersonic vehicle developed at NASA Langley Research Center is presented in Refs. 1 and 2. The equations of motion include an inverse-square-law gravitational model and the centripetal acceleration for the nonrotating Earth. The longitudinal dynamics of the air vehicle model can be described by a set of differential equations for velocity, flight-path angle, altitude, angle of attack, and pitch rate as

$$\dot{V} = \frac{T\cos\alpha - D}{m} - \frac{\mu \sin\gamma}{r^2} \tag{1}$$

$$\dot{\gamma} = \frac{L + T\sin\alpha}{mV} - \frac{(\mu - V^2 r)\cos\gamma}{Vr^2} \tag{2}$$

$$\dot{h} = V\sin\gamma \tag{3}$$

$$\dot{\alpha} = q - \dot{\gamma} \tag{4}$$

$$\dot{q} = \frac{M_{yy}}{I_{yy}} \tag{5}$$

where

$$L = \tfrac{1}{2}\rho V^2 S C_L \tag{6}$$

$$D = \tfrac{1}{2}\rho V^2 S C_D \tag{7}$$

$$T = \tfrac{1}{2}\rho V^2 S C_T \tag{8}$$

$$M_{yy} = \tfrac{1}{2}\rho V^2 S\bar{c}[C_M(\alpha) + C_M(\delta_e) + C_M(q)] \tag{9}$$

$$r = h + R_E \tag{10}$$

The engine dynamics are modeled by a second-order system:

$$\ddot{\beta} = -2\zeta\omega_n\dot{\beta} - \omega_n^2\beta + \omega_n^2\beta_c \tag{11}$$

For the purpose of this study, the aerodynamic coefficients are simplified around the nominal cruising flight. The nominal flight of the vehicle is at a trimmed cruise condition ($M = 15$, $V =$ 15,060 ft/s, $h = 110{,}000$ ft, $\gamma = 0$ deg, and $q = 0$ deg/s). Parametric uncertainty is modeled as an additive variance Δ to the nominal

values used for control design. For illustration, only limited number of uncertain parameters is considered,

$$C_L = 0.6203\alpha \tag{12}$$

$$C_D = 0.6450\alpha^2 + 0.0043378\alpha + 0.003772 \tag{13}$$

$$C_T = \begin{cases} 0.02576\beta & \text{if} \quad \beta < 1 \\ 0.0224 + 0.00336\beta & \text{if} \quad \beta > 1 \end{cases} \tag{14}$$

$$C_M(\alpha) = -0.035\alpha^2 + 0.036617(1 + \Delta C_{M\alpha})\alpha + 5.3261 \times 10^{-6} \tag{15}$$

$$C_M(q) = (\bar{c}/2V)q(-6.796\alpha^2 + 0.3015\alpha - 0.2289) \tag{16}$$

$$C_M(\delta_e) = c_e(\delta_e - \alpha) \tag{17}$$

$$m = m_0(1 + \Delta m) \tag{18}$$

$$I_{yy} = I_0(1 + \Delta I) \tag{19}$$

$$S = S_0(1 + \Delta S) \tag{20}$$

$$\bar{c} = \bar{c}_0(1 + \Delta\bar{c}) \tag{21}$$

$$\rho = \rho_0(1 + \Delta\rho) \tag{22}$$

$$c_e = 0.0292(1 + \Delta c_e) \tag{23}$$

where the nominal values are given by $m_0 = 9375$, $I_0 = 7 \times 10^6$, $S_0 = 3603$, $\bar{c}_0 = 80$, and $\rho_0 = 0.24325 \times 10^{-4}$. The maximum values of the additive uncertainties used in the simulation studies are taken as follows:

$$|\Delta m| \le 0.03, \qquad |\Delta I| \le 0.02, \qquad |\Delta S| \le 0.01$$

$$|\Delta\bar{c}| \le 0.01, \qquad |\Delta\rho| \le 0.06$$

$$|\Delta c_e| \le 0.03, \qquad |\Delta C_{M\alpha}| \le 0.1 \tag{24}$$

The control inputs are the throttle setting β_c and the elevator deflection δ_e. The outputs are the velocity V and the altitude h. The commanded desired values of velocity and altitude are denoted by $V_d(t)$ and $h_d(t)$, respectively.

Input/Output Linearization

The longitudinal model of the generic hypersonic air vehicle described by Eqs. (1–5) is a special case of a general MIMO nonlinear system of the form

$$\dot{\boldsymbol{x}}(t) = \boldsymbol{f}(\boldsymbol{x}) + \sum_{k=1}^{m} \boldsymbol{g}_k(\boldsymbol{x})u_k \tag{25}$$

$$y_i(t) = h_i(\boldsymbol{x}), \qquad i = 1, \ldots, m \tag{26}$$

where $\boldsymbol{f}$, $\boldsymbol{g}$, and $\boldsymbol{h}$ are sufficiently smooth functions of $\boldsymbol{x} \in \Re^n$. Input/output linearization uses full state feedback to globally linearize the nonlinear dynamics of selected controlled outputs. Following the approach in Ref. 4, each of the output channels y_i is differentiated a sufficient number of times until a control input component appears in the resulting equation. Let r_i, the linearizability index, be the minimum order of the derivative of y_i for which the coefficient of at least one u_k is not zero. When the Lie derivative notation is used, this derivative can be expressed as

$$y_i^{(r_i)} = L_f^{r_i}(h_i) + \sum_{k=1}^{m} L_{g_k}\left[L_f^{r_i-1}(h_i)\right]u_k \tag{27}$$

where the Lie derivatives are defined as

$$L_f(h_i) = \frac{\partial h_i}{\partial x_1} f_1 + \cdots + \frac{\partial h_i}{\partial x_n} f_n$$

$$L_f^r(h_i) = L_f\left[L_f^{r-1}(h_i)\right], \qquad L_{g_k}(h_i) = \frac{\partial h_i(\boldsymbol{x})}{\partial \boldsymbol{x}}\boldsymbol{g}_k$$

Given that the nonlinear system is I/O linearizable, for each output y_i there exists a linearizability index r_i. Accordingly,

$$r = \sum_{i=1}^{m} r_i$$

is called the relative degree of the nonlinear system. The necessary and sufficient condition for the existence of a transformation linearizing the system completely from the I/O point of view is that the relative degree r be the same as the order of the system, n, that is, $r = n$. If $r < n$, however, the nonlinear system can only be partially linearized. In this case, the stability of the nonlinear system given by Eqs. (25) and (26) depends not only on the linearized system, but also on the stability of the internal dynamics (zero dynamics).

When the described technique is applied to the longitudinal model of the hypersonic vehicle, the output dynamics for velocity V and altitude h can be derived by differentiating V three times and h four times as shown later. Therefore, the relative degree of the system, $r = 3 + 4 = 7 = n$, equals to the order of the system. Thus, the nonlinear longitudinal model can be linearized completely, and the closed-loop system has no zero dynamics.[2] The linearized model is developed by repeated differentiation of V and h as follows:

$$\dot{V} = f_1(\boldsymbol{x}), \qquad \ddot{V} = \omega_1\dot{\boldsymbol{x}}/m, \qquad \dddot{V} = (\omega_1\ddot{\boldsymbol{x}} + \dot{\boldsymbol{x}}\Omega_2\dot{\boldsymbol{x}})/m \tag{28}$$

$$\dot{h} = \dot{V}\sin\gamma + V\dot{\gamma}\cos\gamma$$

$$\ddot{h} = \ddot{V}\sin\gamma + 2\dot{V}\dot{\gamma}\cos\gamma - V\dot{\gamma}^2\sin\gamma + V\ddot{\gamma}\cos\gamma$$

$$h^{(4)} = \dddot{V}\sin\gamma + 3\ddot{V}\dot{\gamma}\cos\gamma - 3\dot{V}\dot{\gamma}^2\sin\gamma + 3\dot{V}\ddot{\gamma}\cos\gamma - 3V\dot{\gamma}\ddot{\gamma}\sin\gamma - V\dot{\gamma}^3\cos\gamma + V\dddot{\gamma}\cos\gamma \tag{29}$$

In Eq. (29),

$$\dot{\gamma} = f_2(\boldsymbol{x}), \qquad \ddot{\gamma} = \pi_1\dot{\boldsymbol{x}}, \qquad \dddot{\gamma} = \pi_1\ddot{\boldsymbol{x}} + \dot{\boldsymbol{x}}^T\Pi_2\dot{\boldsymbol{x}} \tag{30}$$

where $\boldsymbol{x}^T = [V \ \gamma \ \alpha \ \beta \ h]$, f_1 and f_2 are the short-hand expressions of the right-hand side of Eqs. (1) and (2), respectively, and $\omega_1 = \partial f_1(\boldsymbol{x})/\partial\boldsymbol{x}$, $\Omega_2 = \partial\omega_1/\partial\boldsymbol{x}$, $\pi_1 = \partial f_2(\boldsymbol{x})/\partial\boldsymbol{x}$, and $\Pi_2 = \partial\pi_1/\partial\boldsymbol{x}$. The detailed expressions of ω_1, Ω_2, π_1, and Π_2 are given in the Appendix.

The right-hand sides of Eqs. (28) and (29) involve second derivatives of α and β. The expression of the second derivatives for α and β can be viewed as consisting of two parts: a part that is control relevant and a part that is not,

$$\ddot{\alpha} = \ddot{\alpha}_0 + \left(\frac{c_e\rho V^2 S\bar{c}}{2I_{yy}}\right)\delta_e \tag{31}$$

$$\ddot{\beta} = \ddot{\beta}_0 + \omega_n^2\beta_c \tag{32}$$

where

$$\ddot{\alpha}_0 = \tfrac{1}{2}\rho V^2 S\bar{c}[C_M(\alpha) + C_M(q) - c_e\alpha]/I_{yy} - \dddot{\gamma} \tag{33}$$

$$\ddot{\beta}_0 = -2\zeta\omega_n\dot{\beta} - \omega_n^2\beta \tag{34}$$

When $\ddot{\boldsymbol{x}}_0^T = [\dddot{V} \ \ddot{\gamma} \ \dddot{\alpha}_0 \ \ddot{\beta}_0 \ \dddot{h}]$ is defined, the output dynamics of V and h can be written in a form in which control inputs β_c and δ_e appear explicitly,

$$\dddot{V} = f_V + b_{11}\beta_c + b_{12}\delta_e \tag{35}$$

$$h^{(4)} = f_h + b_{21}\beta_c + b_{22}\delta_e \tag{36}$$

where

$$f_V = \frac{\left(\omega_1 \ddot{\boldsymbol{x}}_0 + \dot{\boldsymbol{x}}^T \Omega_2 \dot{\boldsymbol{x}}\right)}{m} \tag{37}$$

$$f_h = 3\ddot{V}\dot{\gamma}\cos\gamma - 3\dot{V}\dot{\gamma}^2\sin\gamma + 3\dot{V}\ddot{\gamma}\cos\gamma - 3V\dot{\gamma}\ddot{\gamma}\sin\gamma - V\dot{\gamma}^3\cos\gamma + \frac{\left(\omega_1 \ddot{\boldsymbol{x}}_0 + \dot{\boldsymbol{x}}^T \Omega_2 \dot{\boldsymbol{x}}\right)\sin\gamma}{m} + V\cos\gamma\left(\pi_1 \ddot{\boldsymbol{x}}_0 + \dot{\boldsymbol{x}}^T \Pi_2 \dot{\boldsymbol{x}}\right) \tag{38}$$

$$b_{11} = \left(\frac{\rho V^2 S c_\beta \omega_n^2}{2m}\right)\cos\alpha \tag{39}$$

$$b_{12} = -\left(\frac{c_e \rho V^2 S \bar{c}}{2m I_{yy}}\right)\left(T\sin\alpha + \frac{\partial D}{\partial \alpha}\right) \tag{40}$$

$$b_{21} = \left(\frac{\rho V^2 S c_\beta \omega_n^2}{2m}\right)\sin(\alpha+\gamma) \tag{41}$$

$$b_{22} = \left(\frac{c_e \rho V^2 S \bar{c}}{2m I_{yy}}\right)\left[T\cos(\alpha+\gamma) + \left(\frac{\partial L}{\partial \alpha}\right)\cos\gamma - \left(\frac{\partial D}{\partial \alpha}\right)\sin\gamma\right] \tag{42}$$

$$c_\beta = \begin{cases} 0.02576, & \beta < 1 \\ 0.00336, & \beta > 1 \end{cases} \tag{43}$$

$$\frac{\partial D}{\partial \alpha} = \frac{1}{2}\rho V^2 S(1.290\alpha + 0.0043378)$$

$$\frac{\partial L}{\partial \alpha} = \frac{1}{2}\rho V^2 S \times 0.6203$$

Sliding Mode Controller Design

The control design problem is to select a vector $[\boldsymbol{\beta}_c \ \boldsymbol{\delta}_e]^T$ that forces the velocity V and altitude h to track some desired commanded values $V_d(t)$ and $h_d(t)$ in the presence of parametric uncertainty. When the techniques introduced in Ref. 4 are applied, first two decoupled sliding surfaces s_1 and s_2 are defined by

$$s_1 = \left(\frac{\mathrm{d}}{\mathrm{d}t} + \lambda_1\right)^3 \int_0^t e_1(\tau)\,\mathrm{d}\tau, \qquad e_1(t) = V - V_d \tag{44}$$

$$s_2 = \left(\frac{\mathrm{d}}{\mathrm{d}t} + \lambda_2\right)^4 \int_0^t e_2(\tau)\,\mathrm{d}\tau, \qquad e_2(t) = h - h_d \tag{45}$$

where λ_1 and λ_2 are strictly positive constants defining the bandwidth of the error dynamics. The sliding surfaces $s_i = 0$, $i = 1, 2$, represent linear differential equations whose solutions imply

$$\int e_i(t), \qquad i = 1, 2$$

approach to zero exponentially with the time constants $2/\lambda_1$ and $3/\lambda_2$, respectively, where the integrals of the tracking errors are used to cancel the steady-state errors.[3]

Differentiating s_1 and s_2, we have

$$\dot{s}_1 = -\dddot{V}_d + f_V + 3\lambda_1\ddot{e}_1 + 3\lambda_1^2\dot{e}_1 + \lambda_1^3 e_1 + b_{11}\boldsymbol{\beta}_c + b_{12}\boldsymbol{\delta}_e \tag{46}$$

$$\dot{s}_2 = -h_d^{(4)} + f_h + 4\lambda_2\ddot{e}_2 + 6\lambda_2^2\ddot{e}_2 + 4\lambda_2^3\dot{e}_2 + \lambda_2^4 e_2 + b_{21}\boldsymbol{\beta}_c + b_{22}\boldsymbol{\delta}_e \tag{47}$$

which can be written in a compact vector form as

$$\begin{bmatrix}\dot{s}_1 \\ \dot{s}_2\end{bmatrix} = \begin{bmatrix}v_1(\boldsymbol{x}, t) \\ v_2(\boldsymbol{x}, t)\end{bmatrix} + \begin{bmatrix}b_{11} & b_{12} \\ b_{21} & b_{22}\end{bmatrix}\begin{bmatrix}\boldsymbol{\beta}_c \\ \boldsymbol{\delta}_e\end{bmatrix} \tag{48}$$

where

$$v_1(\boldsymbol{x}, t) = -\dddot{V}_d + f_V + 3\lambda_1\ddot{e}_1 + 3\lambda_1^2\dot{e}_1 + \lambda_1^3 e_1 \tag{49}$$

$$v_2(\boldsymbol{x}, t) = -h_d^{(4)} + f_h + 4\lambda_2\ddot{e}_2 + 6\lambda_2^2\ddot{e}_2 + 4\lambda_2^3\dot{e}_2 + \lambda_2^4 e_2 \tag{50}$$

The sliding control design is then choosing the control inputs such that the following attractive equations are satisfied:

$$\frac{1}{2}\frac{\mathrm{d}s_1^2}{\mathrm{d}t} \le -k_1|s_1| \tag{51}$$

$$\frac{1}{2}\frac{\mathrm{d}s_2^2}{\mathrm{d}t} \le -k_2|s_2| \tag{52}$$

where k_1 and k_2 are strictly positive constants that determine the desired reaching time to the sliding surfaces. The attractive Eqs. (51) and (52), also called sliding conditions, imply that the distance to the sliding surface decreases along all system trajectories. Furthermore, the sliding condition makes the sliding surfaces an invariant set, that is, once a system trajectory reaches the surface, it will remain on it for the rest of the time. In addition, for any initial condition, the sliding surface will be reached in a finite time.[3]

When Eq. (48) is used, the controller that satisfies the sliding conditions (51) and (52) can be chosen as

$$\begin{bmatrix}\boldsymbol{\beta}_c \\ \boldsymbol{\delta}_e\end{bmatrix} = \boldsymbol{B}^{-1}\begin{bmatrix}-v_1(\boldsymbol{x}, t) - k_1\,\mathrm{sgn}(s_1) \\ -v_2(\boldsymbol{x}, t) - k_2\,\mathrm{sgn}(s_2)\end{bmatrix}, \qquad \boldsymbol{B} = \begin{bmatrix}b_{11} & b_{12} \\ b_{21} & b_{22}\end{bmatrix} \tag{53}$$

where $\boldsymbol{B}$ is assumed to be invertible. It is easy to see that $\boldsymbol{B}$ inverse does indeed exist for the entire flight envelope except on a vertical flight path.[2] The control law (53) can be viewed as consisting of two parts: the term $-\boldsymbol{B}^{-1}[v_1 \ v_2]^T$, called the equivalent control, which guarantees $\dot{s}_i = 0$, $i = 1, 2$, for the nominal model, and the other term $-\boldsymbol{B}^{-1}[k_1\mathrm{sgn}(s_1) \ k_2\mathrm{sgn}(s_2)]$, incorporated to deal with parameter uncertainties. With this design, the sliding surfaces will be reached even in the presence of parameter uncertainties. In fact, in the presence of parameter uncertainty, one has

$$\begin{bmatrix}\dot{s}_1 \\ \dot{s}_2\end{bmatrix} = \begin{bmatrix}\Delta f_V + v_1 \\ \Delta f_h + v_2\end{bmatrix} + (\Delta\boldsymbol{B} + \boldsymbol{B})\boldsymbol{B}^{-1}\begin{bmatrix}-v_1 - k_1\,\mathrm{sgn}(s_1) \\ -v_2 - k_2\,\mathrm{sgn}(s_2)\end{bmatrix} \tag{54}$$

As discussed in Ref. 3, when large enough k_1 and k_2 are chosen, the sliding conditions (51) and (52) can be satisfied. However, because of the discontinuity across the sliding surfaces, the preceding control law may result in control chattering. As a practical matter, chattering is undesirable because it involves very high control action and may excite high-frequency dynamics neglected in the modeling. The discontinuity in the control law can be dealt with by defining two thin boundary layers of widths Φ_1 and Φ_2 around the sliding surfaces, that is, replacing $\mathrm{sgn}(s_i)$ with continuous saturation functions $\mathrm{sat}(s_i/\Phi_i)$, $i = 1, 2$, where $\mathrm{sat}(x) = x$ if $|x| \le 1$ and $\mathrm{sat}(x) = \mathrm{sgn}(x)$ otherwise. Therefore, our sliding controller is modified as follows:

$$\begin{bmatrix}\boldsymbol{\beta}_c \\ \boldsymbol{\delta}_e\end{bmatrix} = \boldsymbol{B}^{-1}\begin{bmatrix}-v_1(\boldsymbol{x}, t) - k_1\,\mathrm{sat}(s_1/\Phi_1) \\ -v_2(\boldsymbol{x}, t) - k_2\,\mathrm{sat}(s_2/\Phi_2)\end{bmatrix} \tag{55}$$

With this scheme, the control law achieves a tradeoff between tracking precision and robustness. Analysis demonstrated by simulations shows that both the sliding surfaces and the attractive conditions influence how fast the system responds to a step input.[4]

Also, to guarantee closed-loop stability, it is necessary to identify the condition where the maximum effect of the combined parameter uncertainties is encountered. Both analytical and simulation studies conducted revealed that the closed-loop system is far more sensitive to variation in the gain matrix $\Delta\boldsymbol{B}$ than it is to Δf_V and Δf_h. To calculate $\Delta\boldsymbol{B}$ for the worst case, the gain matrix is written as a

product of a fixed basis matrix Y and an uncertainty parameter matrix,

$$\boldsymbol{B} = \begin{bmatrix} (1/a)Y_{11} & (1/b)Y_{12} \\ (1/a)Y_{21} & (1/b)Y_{22} \end{bmatrix} = \begin{bmatrix} Y_{11} & Y_{12} \\ Y_{21} & Y_{22} \end{bmatrix} \begin{bmatrix} (1/a) & 0 \\ 0 & (1/b) \end{bmatrix} \quad (56)$$

where

$$a = \frac{2 \times 10^{-4} m}{\rho S c_\beta \omega_n^2} \quad (57)$$

$$b = \frac{4 \times 10^{-14} I_{yy} m}{\rho^2 S^2 c_e \bar{c}} \quad (58)$$

$$Y_{11} = V^2 \cos\alpha \times 10^{-4} \quad (59)$$

$$Y_{21} = V^2 \sin(\alpha + \gamma) \times 10^{-4} \quad (60)$$

$$Y_{12} = -V^4 \left(C_T \sin\alpha + \frac{\partial C_D}{\partial \alpha} \right) \times 10^{-14} \quad (61)$$

$$Y_{22} = V^4 \left\{ C_T \cos(\alpha + \gamma) + \left(\frac{\partial C_L}{\partial \alpha} \right) \cos\gamma - \left(\frac{\partial C_D}{\partial \alpha} \right) \sin\gamma \right\} \times 10^{-14} \quad (62)$$

Constants a and b embody the combinations of all uncertainty parameters in $\boldsymbol{B}$. The worst case occurs when Δm and ΔI take their maximum negative values, while $\Delta\rho$, ΔS, Δc_e, and $\Delta\bar{c}$ take their maximum positive values. In this study, the nominal values of a and b are 1.1926 ft · s^2 and 0.1463 ft^3/s, and the true values of a and b are 1.0805 ft · s^2 and 0.1166 ft^3/s, respectively. Therefore, the parameter a contains 10.4% uncertainty and the parameter b contains 25.4% uncertainty. In a hypersonic vehicle, these uncertainties are significant. The uncertainties in f_V and f_h are nonlinear combinations of the uncertainty in parameters. When a Taylor series expansion of these terms around their nominal values is used and the high-order error terms are neglected, the terms Δf_V and Δf_h can be estimated from their nominal values.

The simulation results are shown in Figs. 1–4. Figures 1 and 2 show the response of the nominal model, that is, no parameter uncertainty. In the simulation studies for the nominal model, k_1 and k_2 are both taken as 2, and Φ_1 and Φ_2 are both chosen as 0.1. Figure 1 shows the vehicle response to a 100-ft/s step-velocity command at the trimmed condition. It is observed that the velocity converges to the desired value in a short time, whereas the altitude remains almost unchanged. Figure 2 shows the vehicle response to a 2000-ft step-altitude command. Similarly, the altitude converges to its desired value with a short response time. In both cases, the controller

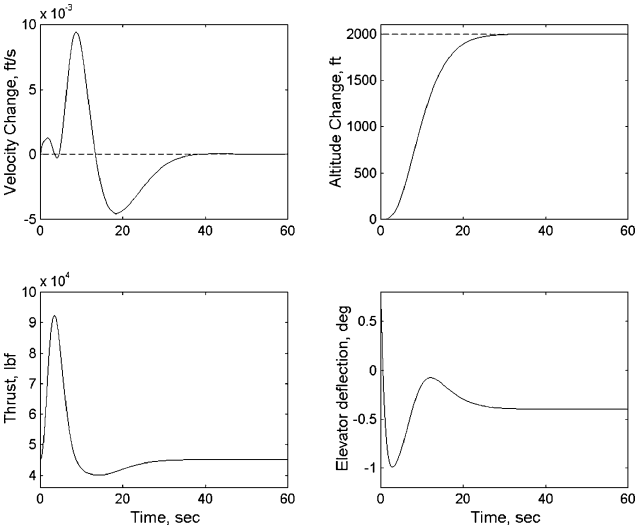

Fig. 2 Response to a 2000-ft step-altitude command for the nominal model.

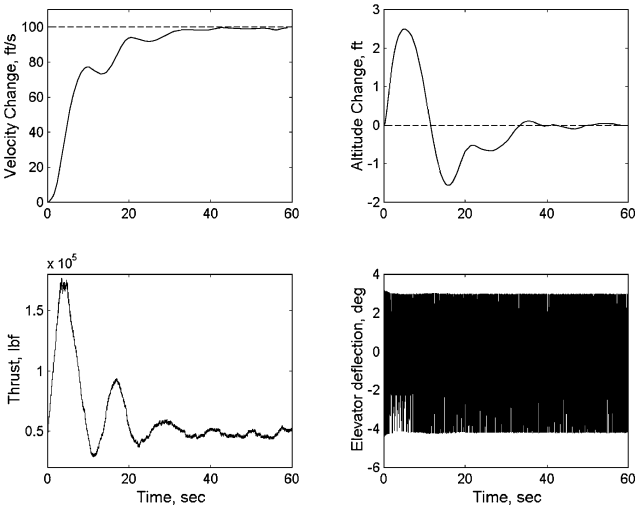

Fig. 3 Response to a 100-ft/s step-velocity command with parameter uncertainties.

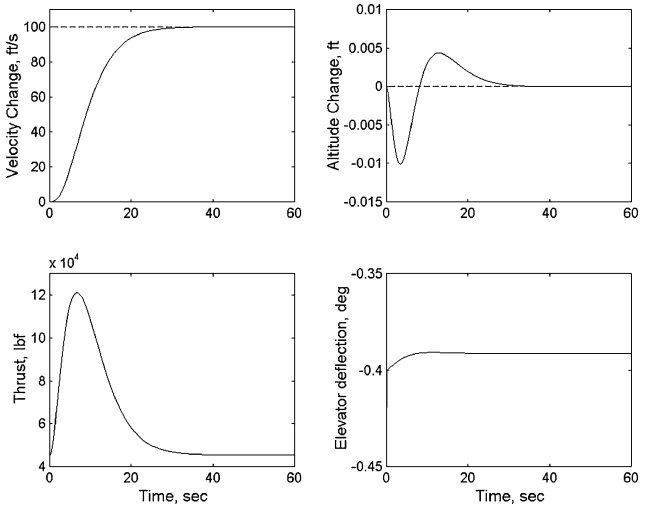

Fig. 1 Response to a 100-ft/s step-velocity command for the nominal model.

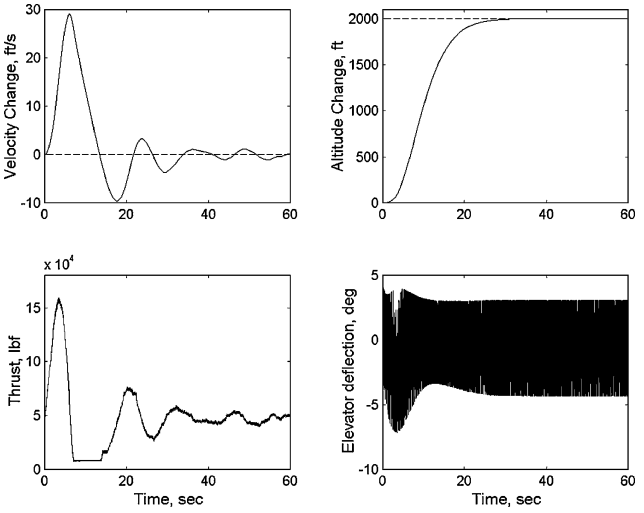

Fig. 4 Response to a 2000-ft step-altitude command with parameter uncertainties.

achieves quick convergence, no overshoot and no steady-state error, for the nominal model. Figures 3 and 4 show the simulation results for the same maneuvers albeit in the presence of parameter uncertainty for the worst case discussed earlier. In this case, k_1 and k_2 are taken as 1400 and 100, and Φ_1 and Φ_2 are chosen as 0.8 and 0.6, respectively. The results show that robustness and stability have indeed been achieved. The price paid to achieve robustness in this case is in the form of large gains k_1 and k_2 and control chattering. However, the control gains cannot be chosen arbitrary large due to practical considerations such as reaching control surface deflection limits. Furthermore, control chattering is undesirable in practice because it involve high control activity and may excite high-frequency unmodeled dynamics. In simulation, the widths of the boundary layers have expanded to reduce chattering. To eliminate chattering, the widths of the boundary layers have to be further expanded, which will result in large steady-state errors. Therefore, in the presence of large parameter uncertainty, pure sliding mode controller requires a tradeoff between steady-state error and control chattering. This drawback of the sliding mode controller is addressed in the next section, where an online parameter estimator is combined with the sliding mode controller to improve performance when parameter uncertainty is present.

Adaptive Sliding Mode Controller Design

As demonstrated in the preceding section, the sliding mode controller achieves good tracking in the presence of parametric uncertainty at the expense of high gains and control chattering. The performance of the sliding mode controller is dependent on the size of the parametric uncertainties involved. An undesirable characteristic of this controller is the quick erosion of performance to gain robustness. This shortcoming of the pure sliding controller has motivated combining the earlier given control law with online parameter adaptation. In this section, we develop an adaptive sliding mode controller that combines an online parameter estimator with the sliding mode controller of the preceding section. The adaptive laws for updating parameters are generated using the Lyapunov synthesis approach (see Ref. 9). As mentioned before, the dynamics of the system is more sensitive to the uncertainty parameters in the gain matrix $\boldsymbol{B}$. The gain matrix $\boldsymbol{B}$ itself is the product of a fixed basis matrix $\boldsymbol{Y}$ and a diagonal matrix with two parameters a and b involving uncertainties. The constant a embodies the combination of a number of uncertain parameters including S, ρ, I_{yy}, and m, and the constant b embodies the combination of uncertain parameters $\bar{c}$, S, c_e, ρ, I_{yy}, and m. For a hypersonic vehicle, these parameters are fixed and strictly positive but difficult to measure exactly at any given time. To deal with the parametric uncertainty, we combine the sliding mode controller with an online parameter estimator forming an adaptive sliding mode controller,

$$\begin{bmatrix} \beta_c \\ \delta_e \end{bmatrix} = \begin{bmatrix} \hat{a} & 0 \\ 0 & \hat{b} \end{bmatrix} \begin{bmatrix} Y_{11} & Y_{12} \\ Y_{21} & Y_{22} \end{bmatrix}^{-1} \bar{\boldsymbol{u}} \tag{63}$$

$$\bar{\boldsymbol{u}} = \begin{bmatrix} -v_1(\boldsymbol{x}, t) - k_1 \operatorname{sat}(s_1/\Phi_1) \\ -v_2(\boldsymbol{x}, t) - k_2 \operatorname{sat}(s_2/\Phi_2) \end{bmatrix} \tag{64}$$

where $\hat{a}$ and $\hat{b}$ are the online estimates of the uncertain parameters a and b.

The adaptive laws can be derived using the Lyapunov synthesis approach. Consider the Lyapunov-like function,

$$V = \tfrac{1}{2}\boldsymbol{s}_\Delta^T \boldsymbol{s}_\Delta + (1/2ak_a)\tilde{a}^2 + (1/2bk_b)\tilde{b}^2 \tag{65}$$

where

$$\tilde{a} = \hat{a} - a, \qquad \tilde{b} = \hat{b} - b, \qquad \boldsymbol{s}_\Delta^T = [s_{1\Delta} \quad s_{2\Delta}]$$

$$s_{1\Delta} = s_1 - \Phi_1 \operatorname{sat}(s_1/\Phi_1), \qquad s_{2\Delta} = s_2 - \Phi_2 \operatorname{sat}(s_2/\Phi_2)$$

where Φ_1 and Φ_2 are two small positive constants. In this construction, $\boldsymbol{s}_\Delta$ can be thought of a measure of the algebraic distances of the current states to the boundary layers. The adaptation ceases as the states reach the boundary layers to avoid parameter estimate drifting.[5] Following the treatment in Ref. 9, we have

$$\dot{V} = \boldsymbol{s}_\Delta^T \begin{bmatrix} -\Delta f_V - k_1 \operatorname{sat}\left(\dfrac{s_1}{\Phi_1}\right) \\ -\Delta f_h - k_2 \operatorname{sat}\left(\dfrac{s_2}{\Phi_2}\right) \end{bmatrix} + \boldsymbol{s}_\Delta^T \begin{bmatrix} Y_{11} & Y_{12} \\ Y_{21} & Y_{22} \end{bmatrix} \begin{bmatrix} \dfrac{\tilde{a}}{a} & 0 \\ 0 & \dfrac{\tilde{b}}{b} \end{bmatrix}$$

$$\times \begin{bmatrix} Y_{11} & Y_{12} \\ Y_{21} & Y_{22} \end{bmatrix}^{-1} \bar{\boldsymbol{u}} + \frac{1}{ak_a}\tilde{a}\dot{\hat{a}} + \frac{1}{bk_b}\tilde{b}\dot{\hat{b}} \tag{66}$$

Equation (66) can be further expanded as

$$\dot{V} = -(k_1 - |\Delta f_V|)|s_{1\Delta}| - (k_2 - |\Delta f_h|)|s_{2\Delta}| + \frac{\tilde{a}}{a}\frac{1}{\Delta}\boldsymbol{s}_\Delta^T$$

$$\times \begin{bmatrix} Y_{11}Y_{22} & -Y_{11}Y_{12} \\ Y_{21}Y_{22} & -Y_{21}Y_{12} \end{bmatrix} \bar{\boldsymbol{u}} + \frac{\tilde{b}}{b}\frac{1}{\Delta}\boldsymbol{s}_\Delta^T \begin{bmatrix} -Y_{12}Y_{21} & Y_{11}Y_{12} \\ -Y_{22}Y_{21} & Y_{11}Y_{22} \end{bmatrix} \bar{\boldsymbol{u}}$$

$$+ \frac{1}{ak_a}\tilde{a}\dot{\hat{a}} + \frac{1}{bk_b}\tilde{b}\dot{\hat{b}}$$

Then, the adaptive laws for estimating uncertain parameters can be derived as

$$\dot{\hat{a}} = -\frac{k_a}{\Delta}\boldsymbol{s}_\Delta^T \begin{bmatrix} Y_{11}Y_{22} & -Y_{11}Y_{12} \\ Y_{21}Y_{22} & -Y_{21}Y_{12} \end{bmatrix} \bar{\boldsymbol{u}} \tag{67}$$

$$\dot{\hat{b}} = -\frac{k_b}{\Delta}\boldsymbol{s}_\Delta^T \begin{bmatrix} -Y_{12}Y_{21} & Y_{11}Y_{12} \\ -Y_{22}Y_{21} & Y_{11}Y_{22} \end{bmatrix} \bar{\boldsymbol{u}} \tag{68}$$

where $\Delta = Y_{11}Y_{22} - Y_{12}Y_{21}$ is the determinant of the matrix $\boldsymbol{Y}$. The sliding gains are chosen as $k_1 \geq |\Delta f_V|_{\max} + l_1$ and $k_2 > |\Delta f_h|_{\max} + l_2$ (where l_1 and l_2 are two positive constants) such that $\dot{V} \leq -l_1|s_{1\Delta}| - l_2|s_{2\Delta}|$, which guarantees all trajectories converge to the boundary layers.

The sliding gains of k_1 and k_2 in this case are taken as 150 and 10, respectively, which are much reduced compared with those in the pure sliding mode control. The simulation results using the adaptive sliding mode controller are shown in Figs. 5–8. When these results are compared with the results obtained using the pure sliding mode controller shown in Figs. 3 and 4, a notable improvement in performance is observed. It is seen that the level of the control effort in the adaptive case is significantly smaller. Figures 6 and 8 show that the parameters converge to their true values. In Fig. 6, the true values are $a = 1.0805\ \text{ft}\cdot\text{s}^2$ and $b = 0.1166\ \text{ft}^3/\text{s}$. Initial nominal values in the estimation were $\hat{a}(0) = 1.1926\ \text{ft}\cdot\text{s}^2$ and $\hat{b}(0) = 0.1463\ \text{ft}^3/\text{s}$. In Fig. 8, true values are $a = 1.0805\ \text{ft}\cdot\text{s}^2$ and $b = 0.1166\ \text{ft}^3/\text{s}$.

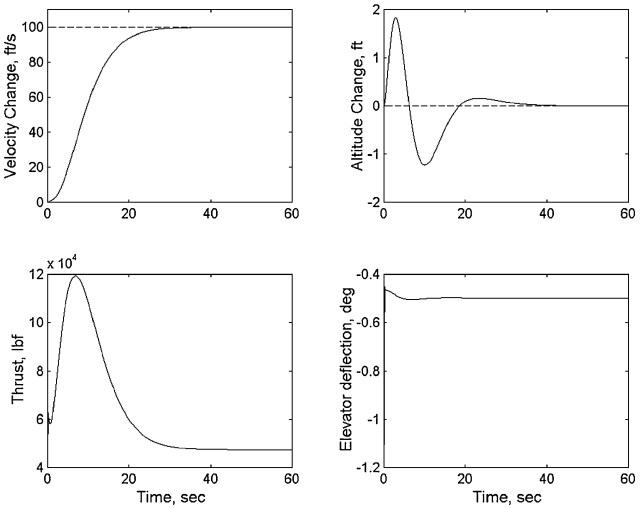

Fig. 5 Adaptive sliding mode controller: response to a 100-ft/s step-velocity command.

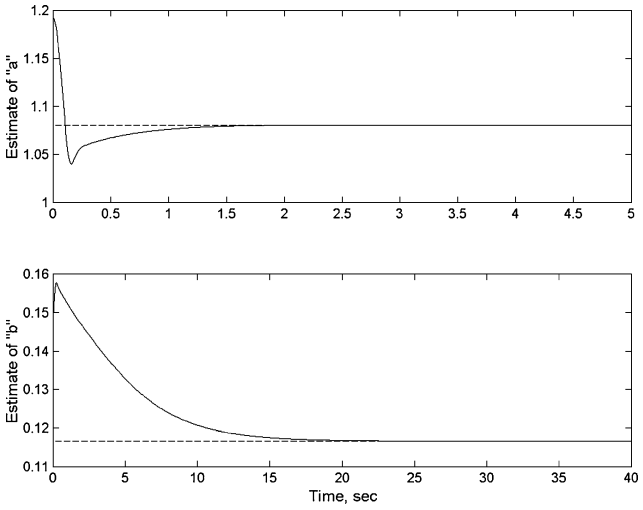

Fig. 6 Parameter estimation in response to a 100-ft/s step-velocity command.

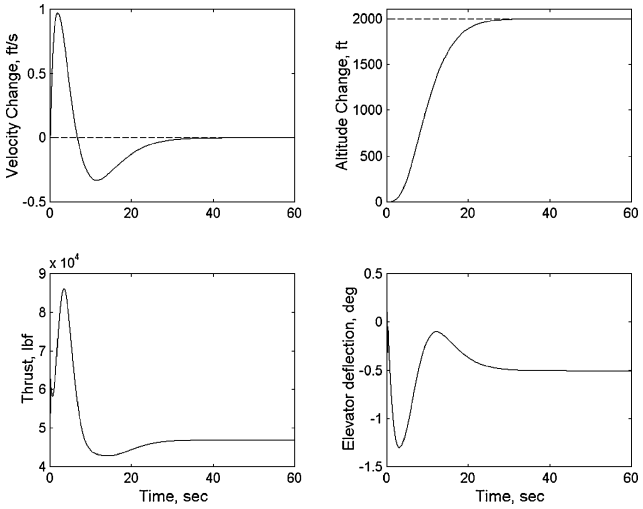

Fig. 7 Adaptive sliding mode controller: response to a 2000-ft step command.

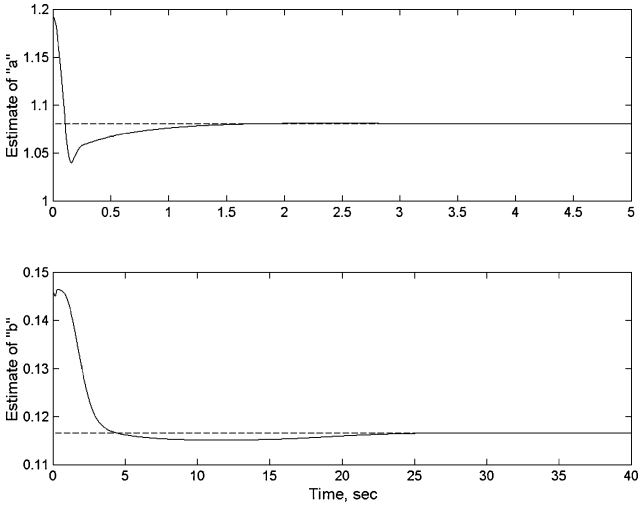

Fig. 8 Parameter estimation in response to a 2000-ft step-altitude command.

Initial nominal values in estimation were $\hat{a}(0) = 1.1926$ ft $\cdot$ s^2 and $\hat{b}(0) = 0.1463$ ft^3/s.

Sliding Mode Observer Design

The sliding mode and the adaptive sliding mode controllers developed in the preceding sections assume that full states are available for measurement. In practice, however, only the states that correspond to velocity V, altitude h, and pitch rate q are expected to be measured. The state variables corresponding to the angle of attack α and flight-path angle γ may be difficult to measure in an actual hypersonic flight because they are generally very small. Accurate measurements are costly and difficult if at all possible to obtain practically. In this section, a sliding mode observer is designed that can provide the estimates of the angle of attack and flight-path angle based on the measurements of velocity, altitude, and pitch rate. When the techniques developed in Ref. 6 are applied, a sliding mode observer is designed whose structure is given by

$$\dot{\hat{h}} = V \sin\hat{\gamma} - \eta_1 \tilde{h} - k_h \mathrm{sgn}(\tilde{h}) \tag{69}$$

$$\dot{\hat{q}} = \frac{\hat{M}_{yy}}{I_0} - \eta_2 \tilde{q} - k_q \mathrm{sgn}(\tilde{q}) \tag{70}$$

$$\dot{\hat{\gamma}} = \frac{\hat{L} + T\sin\hat{\alpha}}{mV} - \frac{(\mu - V^2 r)\cos\hat{\gamma}}{Vr^2} - \eta_3 \tilde{h} - k_\gamma \mathrm{sgn}(\tilde{h}) \tag{71}$$

$$\dot{\hat{\alpha}} = \hat{q} - \dot{\hat{\gamma}} - \eta_4 \tilde{q} - k_\alpha \mathrm{sgn}(\tilde{q}) \tag{72}$$

where

$$\hat{L} = \tfrac{1}{2}\rho_0 V^2 S_0 \times 0.6203\hat{\alpha}$$

$$\hat{M}_{yy} = \tfrac{1}{2}\rho_0 V^2 S_0 \bar{c}_0 \big[(-0.035\hat{\alpha}^2 + 0.036617\hat{\alpha} + 5.3261 \times 10^{-6}) + (\bar{c}_0/2V) q(-6.796\hat{\alpha}^2 + 0.3015\hat{\alpha} - 0.2289) + 0.0292(\delta_e - \hat{\alpha})\big]$$

$$\tilde{h} = \hat{h} - h, \qquad \tilde{q} = \hat{q} - q$$

and where η_1, η_2, η_3, and η_4 are positive constants selected as 2.0, 1.8, 0.0001, and 0.001, respectively, and k_h, k_q, k_γ, and k_α are the sliding gains chosen by the designer.

The sliding surfaces of the observer are defined by $s_0 = 0$, where $s_0 = [\tilde{h}\ \tilde{q}]^T$. The average error dynamics during sliding where $s_0 = 0$ and $\dot{s}_0 = 0$ are

$$\tilde{h} = 0 \tag{73}$$

$$\tilde{q} = 0 \tag{74}$$

$$V(\sin\hat{\gamma} - \sin\gamma) - k_h \mathrm{sgn}(\tilde{h}) = 0 \tag{75}$$

$$\left(\frac{1}{2I_0}\right)\rho_0 V^2 S_0 \bar{c}_0 \left\{-0.035(\hat{\alpha}^2 - \alpha^2) + \left[0.00742 - 0.3015\left(\frac{\bar{c}_0}{2V}\right)q\right]\tilde{\alpha} - 6.796\left(\frac{\bar{c}_0}{2V}\right)q(\hat{\alpha}^2 - \alpha^2)\right\} - k_q \mathrm{sgn}(\tilde{q}) = 0 \tag{76}$$

$$\dot{\tilde{\gamma}} = \frac{0.3102\rho_0 V^2 S_0 \tilde{\alpha} + T(\sin\hat{\alpha} - \sin\alpha)}{mV} - \frac{(\mu - V^2 r)(\cos\hat{\gamma} - \cos\gamma)}{Vr^2} - k_\gamma \mathrm{sgn}(\tilde{h}) \tag{77}$$

$$\dot{\tilde{\alpha}} = -\dot{\tilde{\gamma}} - k_\alpha \mathrm{sgn}(\tilde{q}) \tag{78}$$

where

$$\tilde{\alpha} = \hat{\alpha} - \alpha, \qquad \tilde{\gamma} = \hat{\gamma} - \gamma$$

The preceding error dynamics are nonlinear and difficult to analyze. Further simplification can be made, however, by noting that, in a hypersonic flight, the velocity V is high and the angle of attack α and flight-path angle γ are typically very small, which justifies the following approximations:

$$\sin\alpha \approx \alpha, \qquad \sin\hat{\alpha} \approx \alpha, \qquad \cos\gamma, \qquad \cos\hat{\gamma} \approx 1$$

$$\hat{\alpha}^2, \alpha^2 \approx 0, \qquad (\bar{c}_0/2V)q \approx 0$$

An approximation for the local error dynamics can be derived from the nonlinear error dynamics of Eqs. (73–78) as

$$\tilde{h} = 0 \tag{79}$$

$$\tilde{q} = 0 \tag{80}$$

$$\dot{\tilde{\gamma}} \approx -V\left(\frac{k_\gamma}{k_h}\right)\tilde{\gamma} + \left\{\frac{\left(0.3102\rho_0 V^2 S_0 + T\right)}{mV}\right\}\tilde{\alpha} \tag{81}$$

$$\dot{\tilde{\alpha}} \approx \left\{-0.00371\left(\frac{k_\alpha}{k_q}\right)\left(\frac{\rho_0 V^2 S_0 \bar{c}_0}{I_0}\right) - \frac{\left(0.3102\rho_0 V^2 S_0 + T\right)}{mV}\right\}\tilde{\alpha} + V\left(\frac{k_\gamma}{k_h}\right)\tilde{\gamma} \tag{82}$$

When the trimmed conditions are substituted, the last two error equations can be further simplified as

$$\dot{\tilde{\gamma}} \approx -15060(k_\gamma/k_h)\tilde{\gamma} + 0.0440\tilde{\alpha} \tag{83}$$

$$\dot{\tilde{\alpha}} \approx -\{0.8425(k_\alpha/k_q) + 0.044\}\tilde{\alpha} + 15060(k_\gamma/k_h)\tilde{\gamma} \tag{84}$$

The convergence of $\tilde{\gamma}$ and $\tilde{\alpha}$ depend on the ratios of k_γ/k_h and of k_α/k_q, respectively. As a rule of thumb, the error dynamics of the observer on sliding surfaces $s_0 = 0$ should be much faster than the tracking error dynamics, that is,

$$\min\{15060(k_\gamma/k_h), 0.8425(k_\alpha/k_q)\} \gg \max\{\lambda_1, \lambda_2\}$$

In this study, $\lambda_1 = 0.3$, $\lambda_2 = 0.38$, k_γ/k_h is chosen as 0.001, and k_α/k_q is chosen as 15, thus, placing the poles of the reduced-order error dynamics of Eqs. (83) and (84) at -15.06 and -12.64. The simulation results in Figs. 9 and 10 show the convergence behavior of the off-line observer, that is, it is not being used for the sliding controller. Figure 9 shows that the errors converge to zero fast when no measurement noise is assumed. In Fig. 10, the errors converge close to zero when a measurement noise with zero mean and standard deviation 80 ft and 0.15 deg/s, respectively, is present. The results demonstrate that the sliding observer has good performance and exhibits robustness with respect to measurement noise.

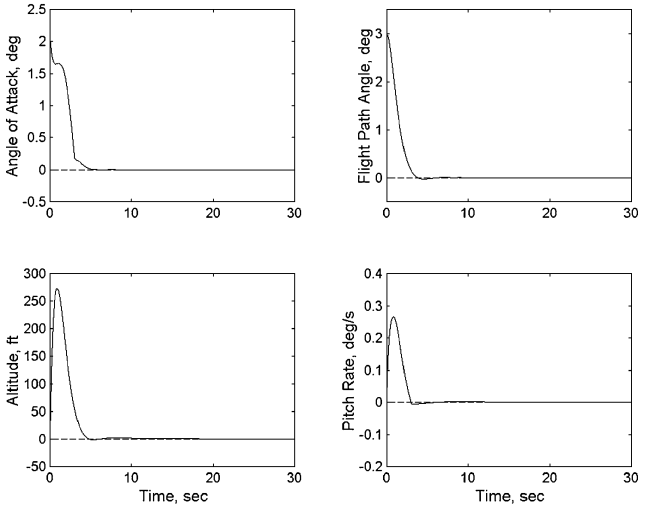

Fig. 9 Off-line sliding observer without measurement noise, initial state errors $\tilde{\gamma}(0) = 3.0$ deg/s and $\tilde{\alpha}(0) = 2.0$ deg.

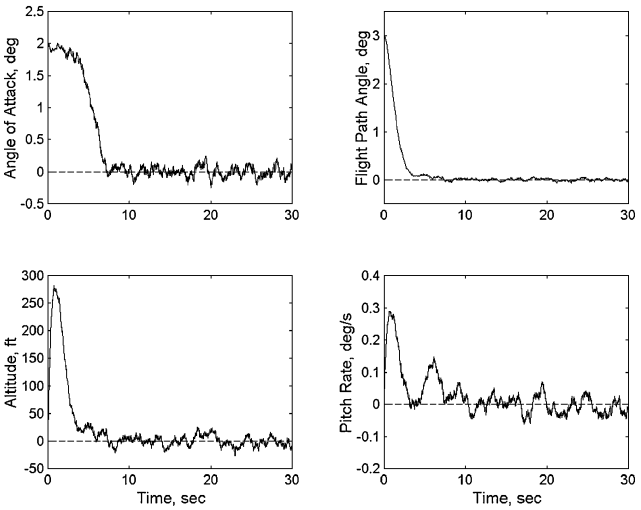

Fig. 10 Off-line sliding observer with Gaussian measurement noise, initial state errors $\tilde{\gamma}(0) = 3.0$ deg/s and $\tilde{\alpha}(0) = 2.0$ deg.

Adaptive Sliding Controller–Observer Synthesis

In the preceding sections we discussed the behavior of the adaptive sliding mode controller and of the sliding mode observer separately. In this section we combine the adaptive sliding mode controller with the observer to synthesize an adaptive sliding mode controller that does not require full state measurement as follows:

$$\hat{\tilde{\boldsymbol{u}}} = \begin{bmatrix} -v_1(\hat{\alpha}, \hat{\gamma}, t) - k_1 \,\mathrm{sat}\left(\dfrac{s_1}{\Phi_1}\right) \\ -v_2(\hat{\alpha}, \hat{\gamma}, t) - k_2 \,\mathrm{sat}\left(\dfrac{s_2}{\Phi_2}\right) \end{bmatrix} \tag{85}$$

$$\begin{bmatrix} \beta_c \\ \delta_e \end{bmatrix} = \begin{bmatrix} \hat{a} & 0 \\ 0 & \hat{b} \end{bmatrix} \begin{bmatrix} Y_{11} & Y_{12} \\ Y_{21} & Y_{22} \end{bmatrix}^{-1} \hat{\tilde{\boldsymbol{u}}} \tag{86}$$

$$\dot{\hat{a}} = -\frac{k_a}{\Delta}\boldsymbol{s}_\Delta^T \begin{bmatrix} Y_{11}Y_{22} & -Y_{11}Y_{12} \\ Y_{21}Y_{22} & -Y_{21}Y_{12} \end{bmatrix} \hat{\tilde{\boldsymbol{u}}} \tag{87}$$

$$\dot{\hat{b}} = -\frac{k_b}{\Delta}\boldsymbol{s}_\Delta^T \begin{bmatrix} -Y_{12}Y_{21} & Y_{11}Y_{12} \\ -Y_{22}Y_{21} & Y_{11}Y_{22} \end{bmatrix} \hat{\tilde{\boldsymbol{u}}} \tag{88}$$

$$\dot{\hat{h}} = V\sin\hat{\gamma} - \eta_1\tilde{h} - k_h\mathrm{sgn}(\tilde{h}) \tag{89}$$

$$\dot{\hat{q}} = \frac{\hat{M}_{yy}}{I_0} - \eta_2\tilde{q} - k_q\mathrm{sgn}(\tilde{q}) \tag{90}$$

$$\dot{\hat{\gamma}} = \frac{\hat{L} + T\sin\hat{\alpha}}{mV} - \frac{(\mu - V^2 r)\cos\hat{\gamma}}{Vr^2} - \eta_3\tilde{h} - k_\gamma\mathrm{sgn}(\tilde{h}) \tag{91}$$

$$\dot{\hat{\alpha}} = \hat{q} - \dot{\hat{\gamma}} - \eta_4\tilde{q} - k_\alpha\mathrm{sgn}(\tilde{q}) \tag{92}$$

where, $v_1(\hat{\alpha}, \hat{\gamma}, t)$ and $v_2(\hat{\alpha}, \hat{\gamma}, t)$ are the same function as $v_1(\boldsymbol{x}, t)$ and $v_2(\boldsymbol{x}, t)$ in which arguments α and γ are replaced by $\hat{\alpha}$ and $\hat{\gamma}$.

The preceding controller is simulated for the same maneuvers and conditions discussed in the preceding sections. The values of k_1 and k_2 are taken as 150 and 10, respectively, which are same as in the adaptive sliding control case. The simulation results are shown in Figs. 11 and 12. It is seen that the adaptive sliding

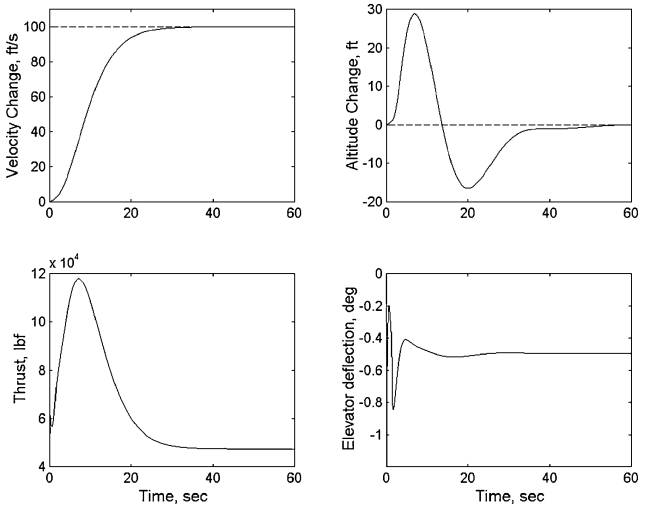

Fig. 11 Adaptive sliding mode controller–observer: response to a 100-ft/s step-velocity command with parameter uncertainties with initial state errors $\tilde{\gamma}(0) = 0.25$ deg/s and $\tilde{\alpha}(0) = 1.5$ deg.

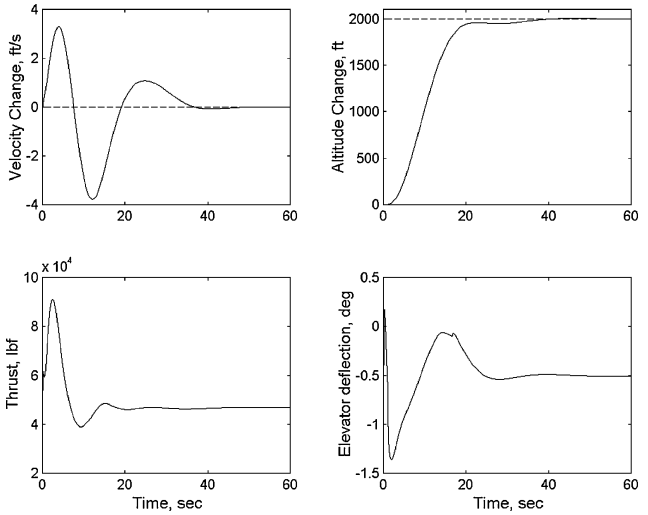

Fig. 12 Adaptive sliding mode controller–observer: response to a 2000-ft step-altitude command with parameter uncertainties with initial state errors $\tilde{\gamma}(0) = 0.25$ deg/s and $\tilde{\alpha}(0) = 1.5$ deg.

mode controller–observer does provide good tracking, despite the presence of parametric uncertainty and assumption of incomplete state measurement.

Conclusions

In this paper, a MIMO adaptive sliding mode controller is designed for the nonlinear longitudinal model of a generic hypersonic vehicle. The controller is developed in several stages. First, a sliding mode controller is developed using full state feedback. Then, the sliding mode controller is made adaptive to deal with parametric uncertainty more efficiently. A nonlinear sliding mode observer is developed to estimate the states that are not available for measurement as in a typical hypersonic flight. The combination of the observer with the adaptive sliding mode controller leads to the final adaptive sliding mode control design that requires only partial state variables to be available for measurement. Simulations conducted demonstrate that the combined adaptive sliding controller–observer has good tracking performance and robustness in the in the presence of parametric uncertainty and the assumption of partial state measurements for the one point in the flight envelop considered in this study.

Appendix

The detailed expressions of the vectors ω_1 and π_1 and matrices Ω_2 and Π_2 are a simplified version of those in Ref. 2:

$$\omega_1^T = \begin{bmatrix} \left(\frac{\partial T}{\partial V}\right)\cos\alpha - \frac{\partial D}{\partial V} \\ \frac{-m\mu\cos\gamma}{r^2} \\ \frac{-T\sin\alpha - \partial D}{\partial\alpha} \\ \left(\frac{\partial T}{\partial\beta}\right)\cos\alpha \\ \frac{2m\mu\sin\gamma}{r^3} \end{bmatrix}$$

$$\pi_1^T = \begin{bmatrix} \frac{\partial L/\partial V + (\partial T/\partial V)\sin\alpha}{mV} & -\frac{L + T\sin\alpha}{mV^2} + \frac{\mu\cos\gamma}{V^2r^2} + \frac{\cos\gamma}{r} \\ & \frac{\mu\sin\gamma}{Vr^2} - \frac{V\sin\gamma}{r} \\ & \frac{\partial L/\partial\alpha + T\cos\alpha}{mV} \\ & \frac{(\partial T/\partial\beta)\sin\alpha}{mV} \\ & \frac{2\mu\cos\gamma}{Vr^3} - \frac{V\cos\gamma}{r^2} \end{bmatrix}$$

$$\Omega_2 = [\omega_{21} \quad \omega_{22} \quad \omega_{23} \quad \omega_{24} \quad \omega_{25}]$$

where

$$\omega_{21} = \begin{bmatrix} \left(\frac{\partial^2 T}{\partial V^2}\right)\cos\alpha - \frac{\partial^2 D}{\partial V^2} \\ 0 \\ -\left(\frac{\partial T}{\partial V}\right)\sin\alpha - \frac{\partial^2 D}{\partial V\partial\alpha} \\ \left(\frac{\partial^2 T}{\partial V\partial\beta}\right)\cos\alpha \\ 0 \end{bmatrix}$$

$$\omega_{22} = \begin{bmatrix} 0 \\ \frac{m\mu\sin\gamma}{r^2} \\ 0 \\ 0 \\ \frac{2m\mu\cos\gamma}{r^3} \end{bmatrix}$$

$$\omega_{23} = \begin{bmatrix} -\left(\frac{\partial T}{\partial V}\right)\sin\alpha - \left(\frac{\partial^2 D}{\partial V\partial\alpha}\right) \\ 0 \\ -T\cos\alpha - \left(\frac{\partial^2 D}{\partial\alpha^2}\right) \\ -\left(\frac{\partial T}{\partial\beta}\right)\sin\alpha \\ 0 \end{bmatrix}$$

$$\omega_{24} = \begin{bmatrix} \left(\dfrac{\partial^2 T}{\partial V \partial \beta}\right)\cos\alpha \\ 0 \\ -\left(\dfrac{\partial T}{\partial \beta}\right)\sin\alpha \\ 0 \\ 0 \end{bmatrix}, \qquad \omega_{25} = \begin{bmatrix} 0 \\ \dfrac{2m\mu\cos\gamma}{r^3} \\ 0 \\ 0 \\ \dfrac{-6m\mu\sin\gamma}{r^4} \end{bmatrix}$$

$$\Pi_2 = [\pi_{21} \quad \pi_{22} \quad \pi_{23} \quad \pi_{24} \quad \pi_{25}]$$

where

$$\pi_{21} = \begin{bmatrix} \dfrac{\partial^2 L/\partial V^2 + (\partial^2 T/\partial V^2)\sin\alpha}{mV} - \dfrac{2[\partial L/\partial V + (\partial T/\partial V)\sin\alpha]}{mV^2} + \dfrac{2(L + T\sin\alpha)}{mV^3} - \dfrac{2\mu\cos\gamma}{V^3 r^2} \\ -\dfrac{\mu\sin\gamma}{V^2 r^2} - \dfrac{\sin\gamma}{r} \\ \dfrac{(\partial^2 L/\partial\alpha\partial V) + (\partial T/\partial V)\cos\alpha}{mV} - \dfrac{\partial L/\partial\alpha + T\cos\alpha}{mV^2} \\ \dfrac{(\partial^2 T/\partial\beta\partial V)\sin\alpha}{mV} - \dfrac{(\partial T/\partial\beta)\sin\alpha}{mV^2} \\ -\dfrac{2\mu\cos\gamma}{V^2 r^3} - \dfrac{\cos\gamma}{r^2} \end{bmatrix}$$

$$\pi_{22} = \begin{bmatrix} -\dfrac{\mu\sin\gamma}{V^2 r^2} - \dfrac{\sin\gamma}{r} \\ \dfrac{\mu\cos\gamma}{Vr^2} - \dfrac{V\cos\gamma}{r} \\ 0 \\ 0 \\ -\dfrac{2\mu\sin\gamma}{Vr^3} + \dfrac{V\sin\gamma}{r^2} \end{bmatrix}, \qquad \pi_{23} = \begin{bmatrix} \dfrac{(\partial^2 L/\partial V\partial\alpha) + (\partial T/\partial V)\cos\alpha}{mV} - \dfrac{\partial L/\partial\alpha + T\cos\alpha}{mV^2} \\ 0 \\ \dfrac{\partial^2 L/\partial\alpha^2 - T\sin\alpha}{mV} \\ \dfrac{(\partial T/\partial\beta)\cos\alpha}{mV} \\ 0 \end{bmatrix}$$

$$\pi_{24} = \begin{bmatrix} \dfrac{(\partial^2 T/\partial V\partial\beta)\sin\alpha}{mV} - \dfrac{(\partial T/\partial\beta)\sin\alpha}{mV^2} \\ 0 \\ \dfrac{(\partial T/\partial\beta)\cos\alpha}{mV} \\ 0 \\ 0 \end{bmatrix}, \qquad \pi_{25} = \begin{bmatrix} -\dfrac{2\mu\cos\gamma}{V^2 r^3} - \dfrac{\cos\gamma}{r^2} \\ -\dfrac{2\mu\sin\gamma}{Vr^3} + \dfrac{V\sin\gamma}{r^2} \\ 0 \\ 0 \\ -\dfrac{6\mu\cos\gamma}{Vr^4} + \dfrac{2V\cos\gamma}{r^3} \end{bmatrix}$$

Acknowledgments

This work was supported in part by the Air Force Office of Scientific Research under Grant F49620-01-1-0489 and in part by NASA Dryden Flight Research Center under Grant NAGA-175.

References

[1]Marrison, C. I., and Stengel, R. F., "Design of Robust Control System for a Hypersonic Aircraft," *Journal of Guidance, Control, and Dynamics*, Vol. 21, No. 1, 1998, pp. 58–62.

[2]Wang, Q., and Stengel, R. F., "Robust Nonlinear Control of a Hypersonic Aircraft," *Journal of Guidance, Control, and Dynamics*, Vol. 23, No. 4, 2000, pp. 577–585.

[3]Slotine, J.-J. E., and Li, W., *Applied Nonlinear Control*, Prentice Hall, Englewood Cliff, NJ, 1991, Chap. 7.

[4]Fernandez, R. B., and Hedrick, J. K., "Control of Multivariable Non-Linear Systems by the Sliding Mode Method," *International Journal of Control*, Vol. 46, No. 3, 1987, pp. 1019–1040.

[5]Slotine, J.-J. E., and Coetsee, J. A., "Adaptive Controller Synthesis for Nonlinear Systems," *International Journal of Control*, Vol. 43, No. 6, 1986, pp. 1631–1651.

[6]Slotine, J.-J. E., Hedrick, J. K., and Misawa, E. A., "On Sliding Observers for Nonlinear Systems," *ASME Journal of Dynamics Systems, Measurement and Control*, Vol. 109, Sept. 1987, pp. 245–252.

[7]Hedrick, J. K., and Yao, W. H., "Adaptive Sliding Control of a Magnetic Suspension System," *Variable Structure Control For Robotics and Aerospace Applications*, edited by K.-K. D. Young, Elsevier Science, New York, 1993, pp. 141–155.

[8]Zak, S. H., Walcott, B. L., and Hui, S., "Variable Structure Control and Observation of Nonlinear/Uncertain Systems," *Variable Structure Control For Robotics and Aerospace Applications*, edited by K.-K. D. Young, Elsevier Science, New York, 1993, pp. 59–88.

[9]Ioannou, P. A., and Sun, J., *Robust Adaptive Control*, Prentice Hall, Upper Saddle River, NJ, 1996.